This is an open access article published under a Creative Commons Attribution (CC-BY) License, which permits unrestricted use, distribution and reproduction in any medium, provided the author and source are cited.

Inorganic Chemistry
Article
pubs.acs.org/IC

Blue-to-Green Emitting Neutral Ir(III) Complexes Bearing Pentafluorosulfanyl Groups: A Combined Experimental and Theoretical Study

Amlan K. Pal,[†,∥] Adam F. Henwood,[†,∥] David B. Cordes,[‡] Alexandra M. Z. Slawin,[‡] Ifor D. W. Samuel,[§] and Eli Zysman-Colman*,[†]

[†]Organic Semiconductor Centre, EaStCHEM School of Chemistry, University of St Andrews, St Andrews, KY16 9ST Fife, U.K.
[‡]EaStCHEM School of Chemistry, University of St Andrews, St Andrews, KY16 9ST Fife, U.K.
[§]Organic Semiconductor Centre, SUPA School of Physics and Astronomy, University of St Andrews, St Andrews, KY16 9SS Fife, U.K.

Supporting Information

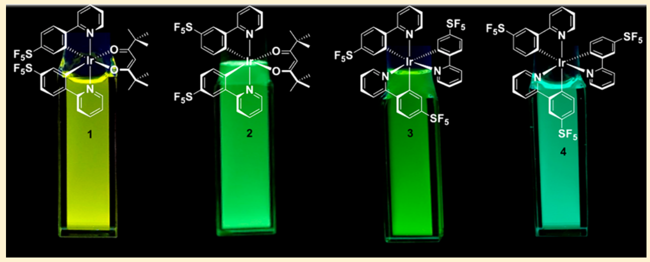

ABSTRACT: A structure−property relationship study of neutral heteroleptic (**1** and **2**, [Ir(C^N)$_2$(L^X)]) and homoleptic (**3** and **4**, *fac*-[Ir(C^N)$_3$]) Ir(III) complexes (where L^X = anionic 2,2,6,6-tetramethylheptane-3,5-dionato-*κO*^{3},*κO*^{6} (thd) and C^N = a cyclometalating ligand bearing a pentafluorosulfanyl (−SF$_5$) electron-withdrawing group (EWG) at the C$_4$ (H**L1**) and C$_3$ (H**L2**) positions of the phenyl moiety) is presented. These complexes have been fully structurally characterized, including by single-crystal X-ray diffraction, and their electrochemical and optical properties have also been extensively studied. While complexes **1** ([Ir(**L1**)$_2$(thd)]), **3** (Ir(**L1**)$_3$), and **4** (Ir(**L2**)$_3$) exhibit irreversible first reduction waves based on the pentafluorosulfanyl substituent in the range of −1.71 to −1.88 V (vs SCE), complex **2** ([Ir(**L2**)$_2$(thd)]) exhibits a quasi-reversible pyridine$_{C^N}$-based first reduction wave that is anodically shifted at −1.38 V. The metal + C^N ligand oxidation waves are all quasi-reversible in the range of 1.08−1.54 V (vs SCE). The optical gap, determined from the lowest energy absorption maxima, decreases from **4** to **2** to **3** to **1**, and this trend is consistent with the Hammett behavior (σ_m/σ_p with respect to the metal−carbon bond) of the −SF$_5$ EWG. In degassed acetonitrile, for complexes **2**−**4**, introduction of the −SF$_5$ group produced a blue-shifted emission (λ_{em} 484−506 nm) in comparison to reference complexes [Ir(ppy)$_2$(acac)] (**R1**, where acac = acetylacetonato) (λ_{em} 528 nm in MeCN), [Ir(CF$_3$-ppy) (acac)] (**R3**, where CF$_3$-ppyH = 2-(4-(trifluoromethyl)phenyl)pyridine) (λ_{em} 522 nm in DCM), and [Ir(CF$_3$-ppy)$_3$] (**R8**) (λ_{em} 507 nm in MeCN). The emission of complex **1**, in contrast, was modestly red shifted (λ_{em} 534 nm). Complexes **2** and **4**, where the −SF$_5$ EWG is substituted para to the Ir−C$_{C^N}$ bond, are efficient phosphorescent emitters, with high photoluminescence quantum yields (Φ_{PL} = 58−79% in degassed MeCN solution) and microsecond emission lifetimes (τ_ε = 1.35−3.02 μs). Theoretical and experimental observations point toward excited states that are principally ligand centered (^{3}LC) in nature, but with a minor metal-to-ligand charge-transfer (^{3}MLCT) transition component, as a function of the regiochemistry of the pentafluorosulfanyl group. The ^{3}LC character is predominant over the mixed ^{3}CT character for complexes **1**, **2**, and **4**, while in complex **3**, there is exclusive ^{3}LC character as demonstrated by unrestricted density functional theory (DFT) calculations. The short emission lifetimes and reasonable Φ_{PL} values in doped thin film (5 wt % in PMMA), particularly for **4**, suggest that these neutral complexes would be attractive candidate emitters in organic light-emitting diodes.

INTRODUCTION

Phosphorescent iridium complexes bearing arylpyridine cyclometalating (C^N) and ancillary ligands (either anionic (L^X) or neutral (L^L)) have gained widespread interest among researchers because of their remarkable optoelectronic properties: e.g., good color tunability, high photoluminescence quantum yields (Φ_{PL}), short emission lifetimes (τ_e), and high photo- and thermostability.[1−3] This confluence of properties render these complexes as attractive candidates as emitters for solid-state electroluminescent devices, the most common of which are organic light-emitting diodes (OLEDs) or light-emitting electrochemical cells (LEECs),[4−7] bioimaging agents,[8,9] and sensing applications.[10] With respect to their use in OLEDs, neutral Ir(III) complexes are generally more desirable in comparison to cationic Ir(III) complexes, as they can be easily vacuum deposited. High-efficiency white flat-panel displays require combined emission from red, green, and blue (RGB) emitters. While the color purity and efficiency of red

Received: April 28, 2017
Published: June 14, 2017

Downloaded via INDIAN INST OF TECH JAMMU on July 31, 2021 at 08:11:57 (UTC).
See https://pubs.acs.org/sharingguidelines for options on how to legitimately share published articles.

Chart 1. Ligands HL1 and HL2 and Neutral Ir(III) Complexes 1−4

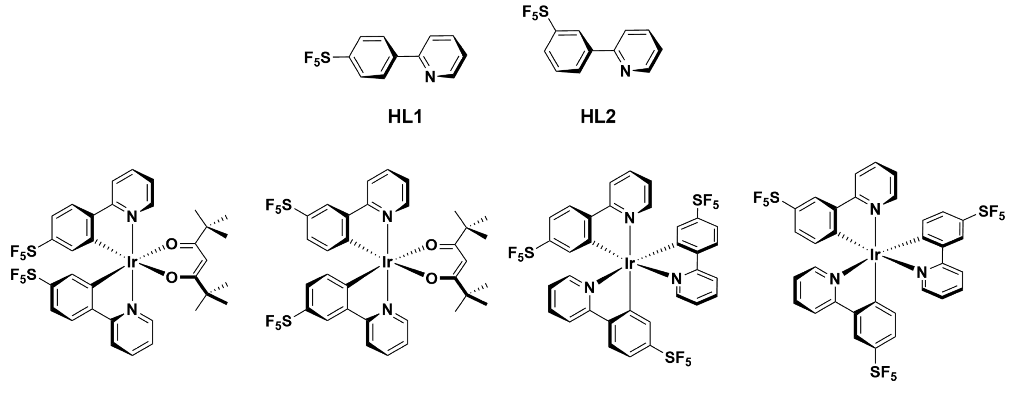

Chart 2. Reference Ir(III) Complexes R1−R10

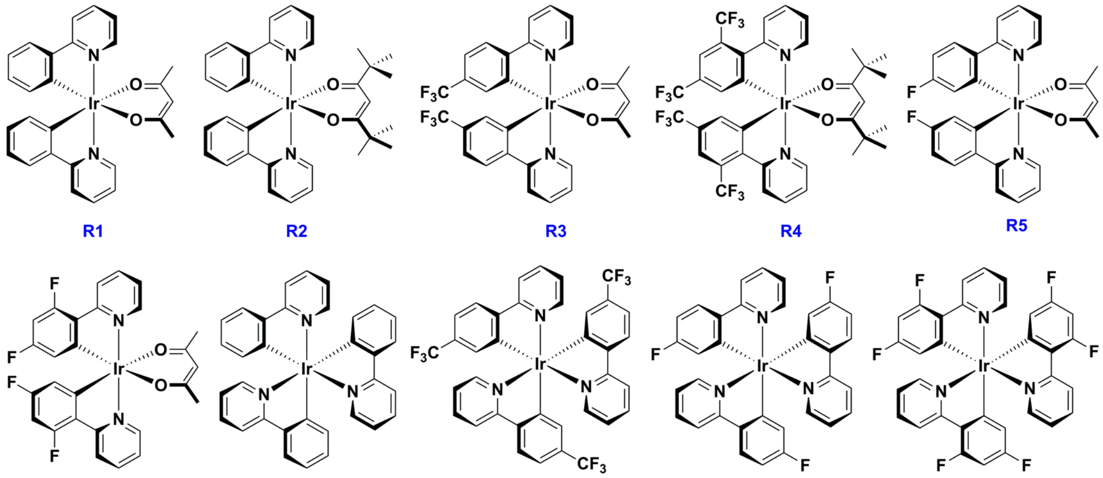

and green Ir(III) emitters are satisfactory, the dearth of high-efficiency blue Ir(III) emitters remains an issue.

Unlike cationic iridium complexes, where color tuning is facile due to independent modulation of the electronics of both the C^N and L^L ligands, for neutral iridium complexes, bearing a nonchromophoric L^X ligand, the emission color is governed by the electronics of the C^N ligands. Substitution of the C^N ligands with EWGs renders the HOMO to be more stabilized than the LUMO. This fact leads to an increased HOMO−LUMO gap, and thus blue emission is achieved. While the near-universal strategy of blue-shifting the emission by incorporation of one or two fluorine atoms in the C^N ligand, such as 2-(4-fluorophenyl)pyridine (FppyH) or 2-(4,6-difluorophenyl)pyridine (dFppyH), is popular,[11−14] the issue of emitter degradation via defluorination negatively affects its incorporation into the emitter design.[15] Apart from fluorine atoms, other examples of EWGs used with a view to blue-shifting the emission of Ir(III) complexes consist of sulfonyl ($-SO_2R$),[16−18] trifluoromethyl ($-CF_3$),[19−23] trifluoromethoxy ($-OCF_3$),[24,25] and pentafluorosulfanyl ($-SF_5$).[26] These C^N ligands are often used in conjunction with nonchromophoric ancillary ligands such as acac,[27] thd,[28] picolinate (pic),[29] and 3-oxo-1,3-diphenylprop-1-en-1-olate (dbm).[30] Although impressive performances have been achieved in solution, translating these performances into devices with good stability and efficiency metrics is still a challenge.[17] Thus, the design and syntheses of new blue-emitting phosphors for OLEDs and LEECs are essential.

Relatively strong intermolecular $\pi-\pi$ interactions are generally observed for planar, nonhindered C^N ligands, leading to the formation of small Ir(III) complex crystallites, which are responsible for unfavorable self-quenching.[31] Incorporation of bulky hydrophobic and chemically inert groups within the C^N ligands leads to the prevention of such aggregate formation, while it also improves the photostability of these complexes in the amorphous phase. Introduction of bulky and strongly electron-withdrawing $-SF_5$ groups (σ_p = 0.68)[32] instead of a trifluoromethyl ($-CF_3$) group (σ_p = 0.54) should lead to significantly blue-shifted emission, concomitant with a blue-shifted absorption, due to stabilization of the C^N-based HOMO. The $-SF_5$ group is strongly electron-withdrawing and has been shown to be lipophilic, thermally and chemically stable, and also biologically active.[33−35] However, despite these favorable properties, as yet it is an underexplored moiety in the field of organic semiconductor materials.[26] Nevertheless, these properties make the $-SF_5$ group an attractive candidate for replacing the commonly used C(aryl)−F motif, serving the same purpose of modulating the HOMO energy but without affecting the stability of the emitter.

The significance of the regiochemistry of the substituent on the C^N ligand in tuning the emission wavelength has been

DOI: 10.1021/acs.inorgchem.7b01075
Inorg. Chem. 2017, 56, 7533−7544

Scheme 1. Synthesis of HL1 and HL2 and Complexes 1−4[a]

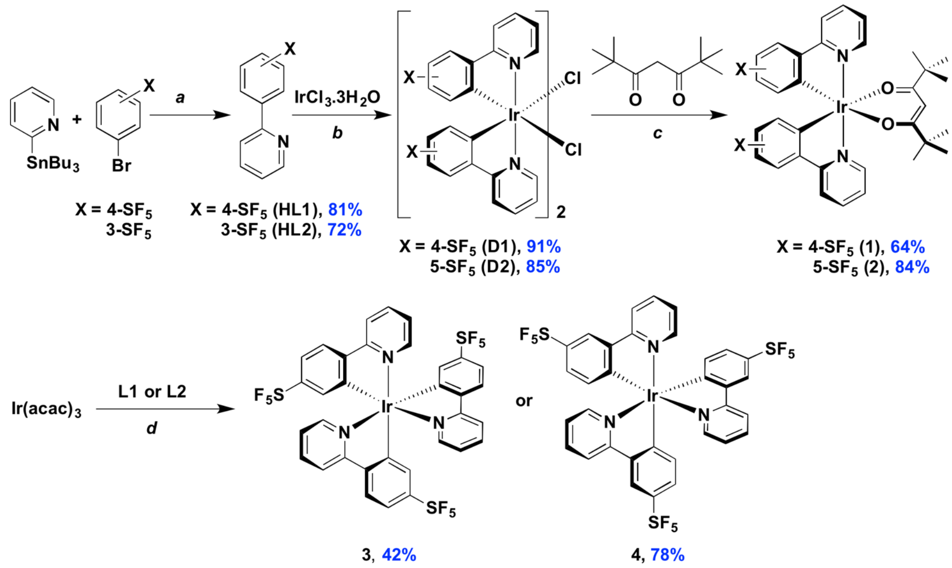

[a]Reagents and conditions. (*a*) 4.6−5.1 mol % of $Pd(PPh_3)_4$, N_2, dry degassed PhMe, 120 °C, 48 h; (*b*) $2\text{-}EtOC_2H_4OH/H_2O$ (3/1 v/v), 120 °C, N_2, 24 h; (*c*) $2\text{-}MeOC_2H_4OH$, anhydrous Na_2CO_3 (2.53 equiv), 110 °C, 24 h, N_2; (*d*) $(CH_2OH)_2$, reflux, N_2, 72 h.

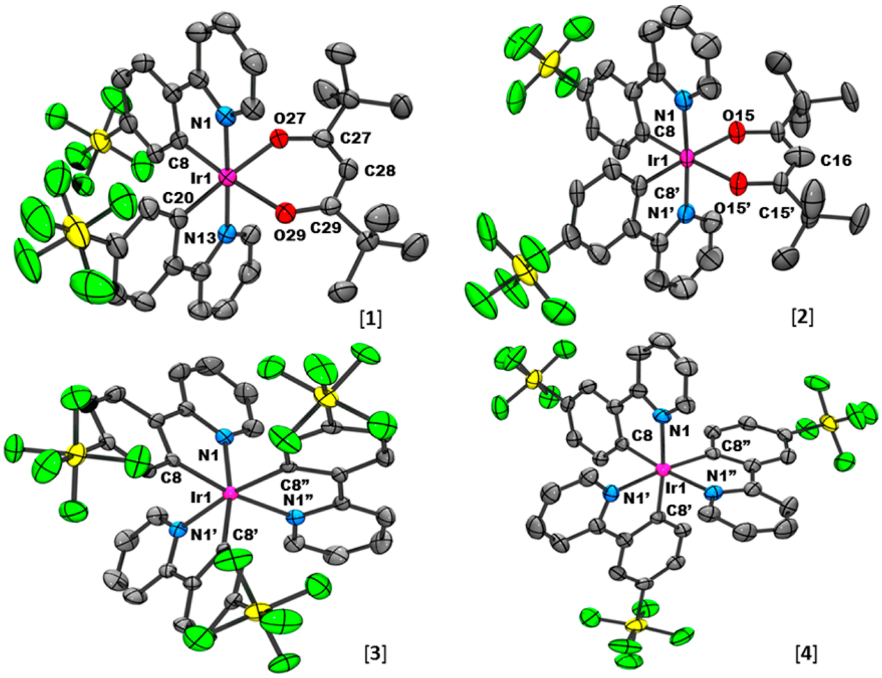

Figure 1. Crystal structures of complexes **1**−**4**. Thermal ellipsoids correspond to a 50% probability level. Hydrogen atoms, solvent molecules, and additional independent molecules are omitted for clarity.

demonstrated by molecular orbital analyses using density functional theory (DFT) calculations.[36,37] For example, the absorption and emission spectra of an Ir(III) complex bearing dFppy C^N ligands (dFppyH = 2-(2,4-difluorophenyl)-pyridine) are more blue-shifted in comparison to an analogous Ir complex with ppy C^N ligands due to greater HOMO stabilization in comparison to LUMO stabilization. When the fluorine atom is located at the 5-position on the C^N ligands (*para* to the Ir−C_{C^N} bond), its inductive electron-withdrawing effect is counterbalanced by weak π donation, thereby raising the HOMO and reducing the band gap.[38]

In a recent study, we investigated the optoelectronic properties of cationic Ir(III) complexes bearing an $-SF_5$ EWG on ppy or phenylpyrazole (ppz) C^N ligands,[26] with the substituent position of the EWG varied so as to adopt either a *para* or *meta* relationship with respect to the Ir−C_{C^N} bond. In this work, a family of neutral emissive Ir(III) complexes with the $-SF_5$ group attached at the 4- (*para* with respect to the Ir−C_{C^N} bond) or 5-position (*meta* with respect to the Ir−C_{C^N} bond) of the C^N ligands (**HL1** and **HL2**; Chart 1) is reported. To ensure neutrality of these complexes, three anionic ligands were employed: complexes **1** and **2** adopt two anionic C^N ligands and 2,2,6,6-tetramethylheptane-3,5-dionato-*κO*^{3},*κO*^{6}

DOI: 10.1021/acs.inorgchem.7b01075
Inorg. Chem. 2017, 56, 7533−7544

Table 1. Redox Data[a] of Complexes 1−4 (in Degassed MeCN) and Benchmark Complexes R1−R3 and R5−R10

compd	E^{ox} (ΔE_p)/V (mV)	E^{red} (ΔE_p)/V (mV)	ΔE_{redox}[b]/V	E_{HOMO}[c]/eV	E_{LUMO}[c]/eV	$\lvert E_{LUMO-HOMO}\rvert$[c]/eV	Hammett param (σ)	
							σ_m	σ_p
1	1.08 (69)	−1.83 (irr)[d]	2.91	−5.57	−1.93	3.64	0.61	
2	1.54 (75)	−1.38 (69), −1.86 (irr)[d]	2.92	−5.64	−1.80	3.84		0.68
3	1.10 (80)	−1.71 (irr)[d]	2.81	−5.66	−1.88	3.78	0.61	
4	1.20 (59)	−1.88 (irr)[d]	3.08	−5.72	−1.74	3.98		0.68
R1[e]	0.86 (95)	−2.15 (125)	3.01				0	0
R2[f]	0.81			−5.17	−1.51	3.66	0	0
R3[g]	1.07						0.43	
R5[h]	0.91 (100)						0.34	
R6[e]	1.21 (115)	−1.99 (115)	3.20				0.34	
R7[i]	0.76	−2.25	3.01				0	0
R8[j]	1.11	−2.13	3.24				0.43	
R9[j]	1.10	−2.13	3.13				0.34	
R10[i]	1.23	−2.06	3.29				0.34	

[a]Potentials reported vs SCE in MeCN using $[n\text{-}Bu_4N]PF_6$ as the supporting electrolyte. Measurements are recorded at room temperature at a scan rate of 100 mV s^{-1}. The difference between the cathodic (E_{pc}) and anodic (E_{pa}) peak potentials, ΔE_p (millivolts) for quasi-reversible redox waves is given in parentheses. [b]ΔE_{redox} is $\lvert E^{ox} - E^{red}\rvert$. [c]DFT calculated energy in eV. [d]Irreversible; potential is given as E_{pc}. [e]From refs 29 and 46 in DMF (a correction factor of 0.05 V has been applied for direct comparison against SCE to calibrate the values in MeCN). [f]From ref 47 in THF (a correction factor of 0.16 V has been applied for direct comparison against SCE to calibrate the values in MeCN). [g]From ref 21 in DCM (measured using SCE as the standard (a correction factor of 0.06 V has been applied for direct comparison against SCE to calibrate the values in MeCN)). [h]From ref 38 in DMF (a correction factor of 0.05 V has been applied for direct comparison against SCE to calibrate the values in MeCN). [i]From ref 42 in DMF (a correction factor of 0.05 V has been applied for direct comparison against SCE to calibrate the values in MeCN). [j]From ref 22 in MeCN.

(thd) as the ancillary ligand, while complexes **3** and **4** are *fac*-homoleptic complexes containing three C^N ligands (Chart 1). The effect of the meta/para position of the $-SF_5$ EWG with respect to the Ir−C_{C^N} bond on the optoelectronic properties of these complexes is discussed and corroborated on the basis of DFT calculations, with the results compared to several benchmark complexes (complexes **R1**−**R10**; Chart 2).

■ RESULTS AND DISCUSSION

Synthesis. The syntheses of the C^N ligands and the iridium complexes **1**−**4** are shown in Scheme 1. As we reported previously, the C^N ligands were synthesized under Stille[39] palladium-catalyzed cross-coupling conditions in good yields.[40] Ligands **HL1** and **HL2** were reacted with $IrCl_3{\cdot}3H_2O$, and the resulting iridium dimers $[Ir(\mathbf{L1})_2(\mu\text{-}Cl)]_2$ (**D1**) and $[Ir(\mathbf{L2})_2(\mu\text{-}Cl)]_2$ (**D2**) were obtained in good yield and used directly in the next synthetic step.[41] Complexes **1** and **2** were isolated in good yield through cleavage of **D1** and **D2** with the thd ligand under basic conditions. The homoleptic complexes **3** and **4** were synthesized upon reaction of 3.1 equiv of the C^N ligands with 1 equiv of $Ir(acac)_3$.[27] A long reaction time (72 h) at high temperature (200 °C) favors the formation of the thermodynamically stable facial (*fac*) isomer in comparison to the kinetically stable meridional (*mer*) isomer,[27] as observed by ^{1}H NMR spectroscopy. All the neutral complexes were purified by column chromatography. The successful syntheses of complexes **1**-**4** confirm the stability of the $-SF_5$ group toward strong bases and high temperatures in organic alcoholic solvents. For both **3** and **4**, ^{19}F NMR indicated the presence of a small impurity (~2%), which, in light of the satisfactory microanalysis, was inferred to be the *mer* isomer. This impurity could not be removed either by chromatography or by repeated recrystallization. In fact, the formation of an inseparable trace amount of the kinetically stable *mer* isomer during the synthesis of the *fac* isomer is already well documented.[42,43] Recrystallization of **3** and **4** on a small scale provided single crystals, which were found to be the expected *fac* isomer by X-ray crystallography (see Figure 1). Complexes **1**−**4** are stable in the presence of air and moisture and are soluble in common organic solvents such as acetonitrile and dichloromethane.

All ligands, dimers and complexes were characterized by ^{1}H, ^{19}F and ^{13}C NMR spectroscopy (Figures S1−S8 and S9−S28 in the Supporting Information), ESI-HRMS, melting point determination, and elemental analyses. The structures of complexes **1**−**4** were unequivocally determined by single crystal X-ray diffraction and corroborated the C_2 (**1** and **2**) and C_3 (**3** and **4**) symmetry assignments ascribed to the complexes on the basis of the solution-state ^{1}H and ^{19}F NMR. The downfield shift of the proton *ortho* to the cyclometalating carbon atom points toward the electron-withdrawing nature of the $-SF_5$ group on the phenyl ring (Figure S6). A similar downfield shift was also found for the proton *ortho* to the carbon atom that is involved in the C_{ph}−$C_{pyridine}$ bond. The ^{19}F NMR spectra exhibit a doublet for the equatorial fluorine atoms and a pentet for the axial fluorine for the $-SF_5$ group in an intensity ratio of 4:1 as an AB_4 system (Figure S7).[44] The HRMS analyses for **1**−**4** showed the indicative peak of the cation $[M + H]^+$.

Crystal Structures. Crystals of **1**−**4** suitable for X-ray analysis were grown by slow diffusion of an antisolvent (**1**, ethanol; **2**, methanol; **3**, diethyl ether; **4**, hexane) into concentrated solutions of the complexes in dichloromethane (Figure 1). Table S1 in the Supporting Information contains relevant crystallographic parameters, and Table S2 in the Supporting Information compares selected bond distances and angles observed in the crystal to those predicted by DFT calculations. In all cases, the metal ion exhibits a pseudo-octahedral coordination geometry. In the case of the heteroleptic complexes **1** and **2**, the pyridyl nitrogen atoms of the C^N ligands are in a mutually *trans* relationship with respect to each other, as is common for many [Ir(C^N)$_2$(L^X)] complexes, such as **R1**.[29] In the case of the homoleptic complexes, all of the nitrogen atoms are in a *cis* relationship. The average Ir−C_{C^N} (1.995 Å) and Ir−C_{C^N} (2.031 Å) bond

DOI: 10.1021/acs.inorgchem.7b01075
Inorg. Chem. 2017, 56, 7533−7544

distances in **1** and **2** are similar to those in **R1** (Ir−$C_{C^\wedge N}$, 1.991 Å; Ir−$C_{C^\wedge N}$, 2.037 Å) (Table S2). A similar structural picture was found in [Ir(**L1**)$_2$(dtBubpy)][PF_6] in our previous study,[26] where dtBubpy is 4,4′-di-*tert*-butyl-2,2′-bipyridine (average Ir−$C_{C^\wedge N}$ distance 2.053 Å and average Ir−$C_{C^\wedge N}$ distance 2.018 Å). In **1** and **2** the average Ir−O distance (2.123 Å) was found to be longer in comparison to the Ir−$C_{C^\wedge N}$ (1.995 Å) and Ir−$C_{C^\wedge N}$ (2.031 Å) bond distances and was in accordance with the similarly longer Ir−O bond distance (2.159 Å) in the reference complex **R1**. The shorter average Ir−O distances in **1** and **2** in comparison to the average Ir−O distance in **R1** are attributed to a strengthened bond, the result of an effective increase in the hardness of the Ir(III) center due to the presence of the electron-withdrawing $-SF_5$ group. In the case of **3** and **4**, the average Ir−$N_{C^\wedge N}$ distance (2.127 Å) was found to be longer than the Ir−$C_{C^\wedge N}$ distance (2.010 Å). In **1** and **2**, the O−Ir−O bite angle (87.9(3)−88.3(1)°) is wider than that of $C_{C^\wedge N}$−Ir−$N_{C^\wedge N}$ (80.5(3)−80.9(2)°). The bond distances and angles predicted by DFT calculations are consistent with those observed in the crystal structures (Table S2). In all of the complexes, the steric bulk of the *tert*-butyl (complexes **1** and **2**) and $-SF_5$ groups prohibit the formation of any significant $\pi-\pi$ stacking interactions.

Electrochemical Properties. In order to assess the effect of the $-SF_5$ group on the ground-state electronics of complexes **1**−**4**, cyclic (CV) and differential pulse voltammetry (DPV) measurements were undertaken. Degassed MeCN was employed as the solvent, and the redox potentials are referenced with respect to SCE (Fc/Fc^+ = 0.38 V in MeCN).[45] The relevant electrochemical data can be found in Table 1 and Table S3 in the Supporting Information, while the CV and DPV traces are shown in Figure 2 (the full set of redox potentials is detailed in Table S3).

At positive potential, complexes **1**−**4** each display oxidation waves that are quasi-reversible and single electron in nature, in the range of 1.08−1.54 V. DFT calculations indicate that incorporation of the $-SF_5$ EWG results in a stabilization of the HOMOs of **1**−**4** in comparison to reference complex **R2** and that the HOMOs of these complexes are comprised of almost equal contributions from the metal center and the C^N ligands (Figure 3). On the basis of the DFT calculations, and in line with literature precedent of related neutral Ir(III) complexes,[29,42] the first oxidation of complexes **1**−**4** is assigned to abstraction of an electron from the metal-based orbitals (the Ir^{III}/Ir^{IV} redox couple) as well as some contribution from the $C^\wedge N_{phenyl}$ orbitals. The lower calculated HOMO energies for **1** (E_{HOMO} = −5.57 eV), **2** (E_{HOMO} = −5.64 eV), **3** (E_{HOMO} = −5.66 eV), and **4** (E_{HOMO} = −5.72 eV) in comparison to that of **R2** (E_{HOMO} = −5.17 eV) are consistent with the expected stabilization of the C^N phenyl based orbitals by the $-SF_5$ group in comparison to **R2** (Table 1). A significant anodic shift of the oxidation potential of **2** by 460 mV was observed in comparison to that of **1**, which is due to the increasing electron-withdrawing nature of the $-SF_5$ group when it is moved from a *meta* position to a *para* position with respect to the Ir−C bond of the C^N ligands. This observation is also in agreement with the increasing Hammett parameter of the $-SF_5$ group when it is positioned regiospecifically (σ_m = 0.61, σ_p = 0.68); this behavior is less pronounced for the *fac*-homoleptic complexes **3** and **4**. Assuming the oxidation potentials are invariant with respect to solvent, the oxidation potentials of **1** and **2** were found to be more positive in comparison to those of **R1**−**R3** and **R5**, implying that $-SF_5$ is a stronger EWG in comparison to −F and $-CF_3$, coincident with the smaller Hammett parameters of these substituents (Table 1).[32] Assuming the fact that thd is a slightly better donor in comparison to acac, as implied by the slight cathodic shift of the oxidation potential of **R2** in comparison to that of **R1**, complex **R6** has an oxidation potential more positive than that of **1** but a value of $E_{1/2}^{ox}$ lower than that of **2**, suggesting that the electron-withdrawing ability follows the order **L2** > dFppy > **L1**. Complexes **3** and **4** are harder to oxidize in comparison to the *fac*-homoleptic reference complexes **R7**−**R9**, which is in line with the Hammett parameters but are 0.03 V (for **4**) to 0.13 V (for **3**) easier to oxidize in comparison to **R10**.

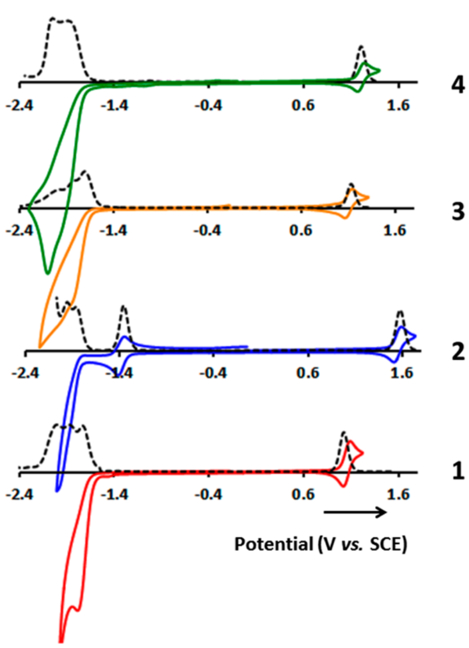

Figure 2. CV (solid) and DPV (dotted) traces of **1**−**4** in deaerated MeCN, recorded at 100 mV s^{-1}.

At negative potentials, multiple ligand-based multielectronic reductions can be observed for **1**−**4** (Figure 2). While for **1**, **3** and **4** the first reductions are irreversible, for **2** this reduction is found to be quasi-reversible and monoelectronic; the second reduction in **2** mirrors the behavior of the first reduction waves for **1**, **3**, and **4**. For **1**, **3**, and **4**, DFT calculations point to a LUMO that has predominant C^N character with significant contribution from the $-SF_5$ group, whereas for **2**, the LUMO remains localized on the C^N ligand but without the contribution from the $-SF_5$ group. Therefore, and in line with our previous results for cationic iridium complexes,[26] the first reduction wave is plausibly assigned to direct reduction of the $-SF_5$ moiety for **1**, **3**, and **4**, where the $-SF_5$ group, upon accepting an electron, may release a fluoride ion, thus rendering the reduction irreversible. Due to the strong electron-withdrawing nature of the $-SF_5$ group, all of the first reduction potentials of **1**−**4** are anodically shifted by between 270 and 770 mV in comparison to that of **R1**. There is a noticeable anodic shift of 0.45 V of the first reduction potential of complex **2** in comparison to that of complex **1**. This reduction wave in **2** is also distinctively reversible and as a consequence does not involve the $-SF_5$ group and in fact represents reduction of the pyridine ring of the C^N ligand. The DFT prediction of the LUMO energy actually aligns well with the second irreversible reduction wave (E^{red2} = −1.86 (irr)). Further, the trend

DOI: 10.1021/acs.inorgchem.7b01075
Inorg. Chem. 2017, 56, 7533−7544

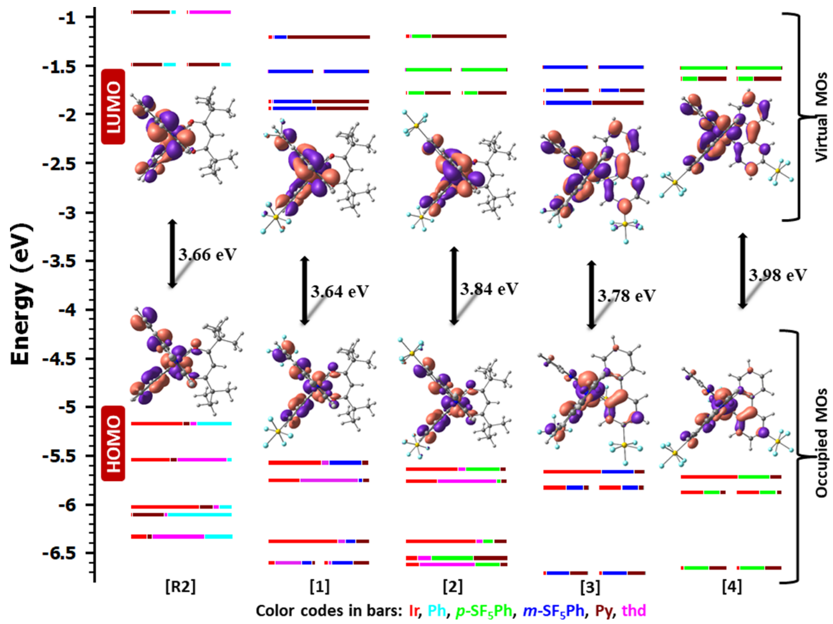

Figure 3. DFT calculated frontier MO energies of **1**–**4** and **R2**, using B3LYP/SBKJC-VDZ for the Ir(III) metal center and 6-31G** for the atoms C, H, N, O, F, and S with CPCM(MeCN) and 0.5 eV threshold of degeneracy (isocontour of 0.03). Kohn–Sham MOs of **1**–**4** and **R2** are also shown.

observed for the DFT-predicted LUMO energies matches the trend in reduction potentials for **1**–**4**, ignoring the reversible reduction wave in **2**. Extrapolated LUMO energies for complexes **1** and **2** ($E_{LUMO(opt)}$ = −3.61 eV for **1** and −4.65 eV for **2**), where $E_{LUMO(opt)} = E^{ox} + \Delta E_{opt}$ and the measured optical gap (ΔE_{opt}) is determined from the energy of the 10% intensity of the lowest energy absorption onset; ΔE_{opt} = 2.53 and 2.81 eV for **1** and **2**, respectively (Figure 4), corroborate

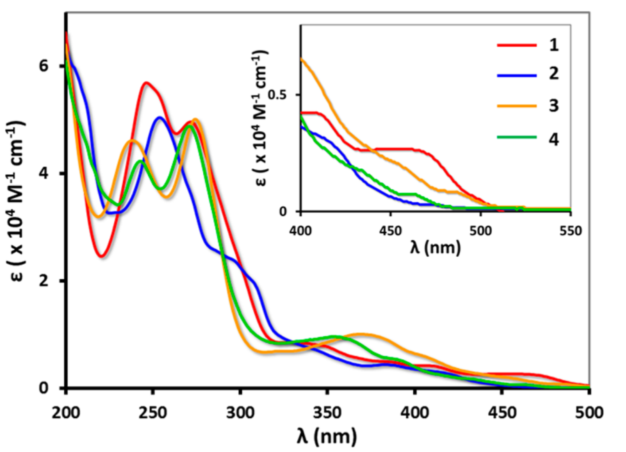

Figure 4. UV–vis absorption spectra of complexes **1**–**4** recorded in MeCN at 298 K (the inset spectrum shows the poorly absorbing bands of complexes **1**–**4** from 400 to 550 nm).

the experimentally determined LUMO energies inferred directly from the electrochemical studies. Thus, DFT calculations for **2** do not predict the reversible pyridine-based reduction and therefore do not accurately predict the LUMO energy for this complex.

Photophysical Properties. The room-temperature UV–vis absorption spectra of **1**–**4** in MeCN are shown in Figure 4, and the data are summarized in Table S4 in the Supporting Information. Figure S29 in the Supporting Information compares the experimentally determined absorption spectra for each of the complexes with the transitions predicted by TD-DFT. The absorption spectra of complexes **1**, **3**, and **4** show two highly absorbing bands between 210 and 300 nm and additional, less absorptive bands beyond 300 nm. For complexes **1** and **2**, prominent spin-allowed $^1\pi \rightarrow \pi^*$ ligand-centered (^{1}LC) transitions localized on the C^N ligand and ligand-to-ligand charge transfer (^{1}LLCT) transitions from the ancillary ligand to the C^N ligands, as predicted by TD-DFT calculations, correlate with the high-energy bands. For complexes **3** and **4**, these bands are $^1\pi \rightarrow \pi^*$ ligand-centered (^{1}LC) transitions as predicted by TD-DFT. The lower energy hypochromic bands between 270 and 300 nm are assigned to a ^{1}LC transition for complexes **3** and **4**, whereas for complexes **1** and **2** these ^{1}LC transitions are mixed with ^{1}MLCT transition contributions (Tables S5–S8 in the Supporting Information). The nature of the transitions between 300 and 400 nm becomes more complex with bands consisting of an admixture of ^{1}LC and ^{1}MLCT transitions, with varying but more significant ^{1}MLCT content along with ligand-to-ligand transitions (^{1}LLCT) in the case specifically for **1** and **2**; the ^{1}LLCT transitions are evidently absent for **3** and **4**. For all of the complexes the band located between 412 and 456 nm is assigned as the HOMO → LUMO transition, which is principally ^{1}MLCT (Ir(dπ) → **L1**/**L2**(π^*)) in nature but mixed with ^{1}LC ($^1\pi \rightarrow \pi^*$) character (Tables S5–S8). Complexes **1**–**4** display a shoulder at λ >450 nm, albeit with very low molar absorptivity, which is a feature also observed for **R1** at 487 nm and **R2** at 468 nm (Table S4).[29,47] These bands are assigned as spin-forbidden ^{3}MLCT and ^{3}LLCT by direct population of the triplet state, which gains intensity by mixing with the higher lying ^{1}MLCT through the strong spin–orbit coupling of the Ir metal center.[48] The spectra observed for **1**–**4** are very similar to those of the corresponding pentafluorosulfanyl-substituted cationic complex [Ir(**L1**)$_2$(dtBubpy)]-[PF$_6$], suggesting that the dominant absorptions in these complexes are due to the "(C^N)$_2$Ir" fragment.[26]

DOI: 10.1021/acs.inorgchem.7b01075
Inorg. Chem. 2017, 56, 7533–7544

The emission spectra in deaerated MeCN solution at room temperature for complexes **1**−**4** are shown in Figure 5a, while Figure 5b shows the doped film (5 wt % in PMMA) emission spectra at room temperature. Table 2 summarizes the relevant solution-phase photophysical data of **1**−**4** as well as the reference complexes **R1**−**R10**. The solid-state photoluminescence data are shown in Table 3. In MeCN solution, the emission of complexes **1**−**4** varies from sky blue to green, with the emission maxima in the range of 484−537 nm. The emission profiles are structured, which is an indication of an excited state that has ^{3}LC character. Spin-unrestricted DFT calculations predict that the spin density is principally localized on a combination of the C^N ligands and the metal center (Figure 6), pointing toward a mixed ^{3}LC and ^{3}MLCT excited state. These predictions are in line with a variety of features that are characteristic of ^{3}LC or ^{3}MLCT emission: the structured vibronic features in the phosphorescence spectra and short (τ_e < 1.5 μs for **1**, **3**, and **4**; τ_e = 3.02 μs for **2**) radiative lifetimes.

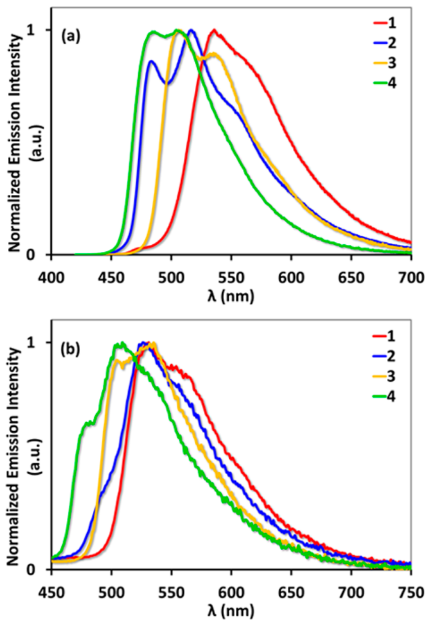

Figure 5. (a) Emission spectra of complexes **1**−**4** in deaerated MeCN at room temperature (λ_{exc} 360 nm). (b) Normalized solid-state photoluminescence spectra of complexes **1**−**4** doped with 5 wt % PMMA.

Table 3. Solid-State Photophysical Data for 1−4 as 5 wt % Doped PMMA Films

compd	λ_{em}/nm	Φ_{PL}/%	τ_e/μs
1	531, 559	35	1.54
2	489, 526, 558	23	1.36
3	507, 535	40	1.18
4	480, 509	51	1.15
R2[a]	518, 570[b], 595[b]	33	
R4[a]	538, 590[b]	49	

[a]From ref 28 as structured emission profiles for both **R2** and **R4**, 4 wt % doped PMMA films. [b]Values of vibronic bands were estimated by visual inspection of the corresponding spectra.

Complex **2** (where the $-SF_5$ EWG is positioned *para* to the Ir−$C_{C\^N}$ bond) exhibits an emission maximum that is blue-shifted in comparison to **1** (where the $-SF_5$ EWG is positioned *meta* to the Ir−$C_{C\^N}$ bond), which fits with the magnitude of the Hammett *meta* and *para* parameters of the $-SF_5$ group. An analogous observation can be made for complexes **3** and **4**. In line with the red shift of the absorption onset from **4** to **2** to **3** to **1** (see inset magnified spectra in Figure 4), the emission maxima are also red-shifted accordingly (Table 2) and this trend also follows the gradually decreasing HOMO−LUMO

Table 2. Relevant Photophysical Data for Complexes 1−4 and Some Benchmark Complexes

		emission[b]				
compd	absorption[a] λ_{abs}/nm (ε/10^3 M^{-1} cm^{-1})	λ_{em}/nm (predicted λ_{em}/nm, relative error/%)	Φ_{PL}/%	τ_e/μs	$10^5 k_r$/s^{-1}	$10^5 k_{nr}$/s^{-1}
1	471 (0.25), 498 (0.05)	534, 563 (sh) (566, 5)	15	0.65	2.31	13.09
2	419 (0.28), 476 (0.07)	484, 516 (521, 4)	79	3.02	2.61	0.69
3	456 (0.19), 489 (0.08)	506, 537 (539, 3)	22	0.61	3.61	12.79
4	435 (0.17), 465 (0.07)	485, 506 (443, 11)	58	1.35	4.29	3.11
R1[c]	456 (0.23), 487 (0.09)	528	34[d]	1.6[c]		
R2[e]	412, 468	525	43			
R3[f]	464 (0.30)	522, 550[g]	32	1.72	1.86	3.95
R4[h]	479 (0.26)	541, 590[g]	43	1.14	3.77	4.99
R5[i]	444 (0.25), 474 (0.08)	493, 560[g]	40	1.5	2.67	4.00
R6[c]	428 (0.20), 458 (0.07)	491	62[j]	0.87[j]		
R7[k]	455 (0.28), 488 (0.16)	518[k]	40	1.9	2.1	3.2
R8[l]	370[g]	507, 540[g]				
R9[l]	358[g]	488				
R10[k]	427 (0.16), 457 (0.03)	468	43	1.6	2.7	3.6

[a]Absorption data are in solvents as mentioned in Table S4 in the Supporting Information. [b]In degassed MeCN at room temperature. Steady-state emission (in MeCN): λ_{exc} 360 nm. Time-resolved emission (in MeCN): λ_{exc} 378 nm. Solution Φ_{PL} values were measured using quinine sulfate as the external reference (λ_{em} 450 nm in MeCN, Φ_r = 54.6% in 0.5 M H_2SO_4 as found in ref 50; the error in prediction of λ_{em} of complexes **1**−**4** were calculated using the equation error = $|[\lambda_{em}(298\ K) - E_{AE}]/\lambda_{em}(298\ K)|$ in eV × 100%, where E_{AE} = adiabatic emission energy). [c]From ref 27 in MeCN (broad and structureless emission profile). [d]From ref 27 in 2-MeTHF. [e]From ref 51 in $CHCl_3$ (broad and structureless emission profile). [f]From ref 21 in DCM (structured emission profile). [g]Values of vibronic bands were estimated by visual inspection of the corresponding spectra. [h]From ref 28 in toluene (structured emission profile). [i]From ref 38 in DCM (structured emission profile). [j]From ref 46 in DCM. [k]From ref 42 in 2-MeTHF (broad and structureless emission profile for **R7** and only emission maximum value is reported for **R10**). [l]From ref 22 in MeCN (structured emission profile for **R8**, broad and structureless emission profile for **R9**).

DOI: 10.1021/acs.inorgchem.7b01075
Inorg. Chem. 2017, 56, 7533−7544

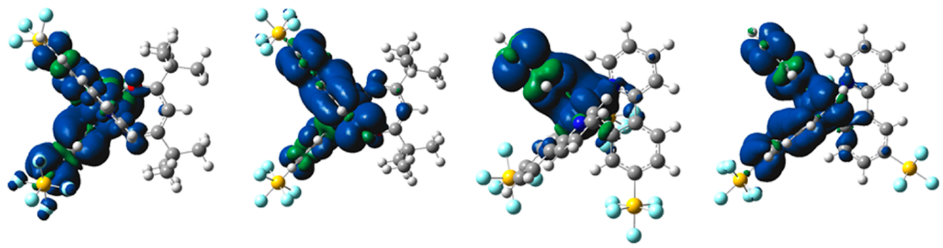

Figure 6. TD-DFT calculated triplet spin density distributions of complexes **1**−**4**, using UB3LYP/SBKJC-VDZ for Ir(III)) and 6-31g** for C, H, N, O, F, and S with CPCM(MeCN). Contours are at an isovalue of 0.02.

gap from **4** to **2** to **3** to **1**, as calculated by DFT (Table 1 and Figure 3). The predicted emission maxima, $E_{AE} = E(T_1) - E(S_0)$ at the T_1 optimized geometries (adiabatic electronic emission) obtained by DFT calculations[36] for **1**−**4**, are respectively, at 566, 521, 539, and 443 nm and match closely those observed experimentally and reproduce the observed trend of red-shifted emission maxima from complex **4** to **2** to **3** to **1**.

Incorporation of the $-SF_5$ EWG on the cyclometalating phenyl rings helps to stabilize the frontier molecular orbitals (Figure 3), leading to a blue shift in the observed emission color for complexes **2**−**4** in comparison to reference complexes **R1** and **R2** (Table 2). For **1**, slight red shifts in its emission maximum in comparison to those of **R1** (6 nm, 213 cm^{-1}) and **R2** (9 nm, 321 cm^{-1}) are observed due to a more stabilized emissive triplet state in **1** in comparison to those in **R1** and **R2**. Considering the fact that ^{3}LC emission is insensitive to solvent polarity,[28] the aforementioned suggestion of a more stabilized triplet state may also be applicable in justifying the observed red shift of the emission maximum of **1** in comparison to those of **R3** and **R5** and thus, surprisingly, are not in line with the Hammett parameters of the substituents (σ_m = 0.61 ($-SF_5$), 0.43 ($-CF_3$), 0.34 (−F)). Complex **R6**, bearing two electron-withdrawing fluorine atoms, displays blue-shifted emission in comparison to that of **1**. Complex **2** with the $-SF_5$ EWG positioned *para* to the Ir−$C_{C^\wedge N}$ bond (σ_p = 0.68 ($-SF_5$)) is bluer than complexes **R1**−**R6**, where there exists *meta* substitution on the C^N ligands with respect to the Ir−$C_{C^\wedge N}$ bond. Likewise, the $-SF_5$ group promotes a more stable emissive triplet state in homoleptic complexes **3** and **4** that is responsible for their observed red shift in the emission maxima (**3** vs **R9** and **R10** and **4** vs **R10**). In comparison to the emission maxima reported in our previous study involving cationic Ir(III) complexes of the form [Ir(**L1**)$_2$(*d*tBubpy)][PF_6] ($\lambda_{em,0-0}$ 482 nm and $\lambda_{em,0-1}$ 517 nm in degassed MeCN) and [Ir(**L2**)$_2$(*d*tBubpy)][PF_6] ($\lambda_{em,0-0}$ 465 nm and $\lambda_{em,0-1}$ 496 nm in degassed MeCN)[26] both the $\lambda_{em,0-0}$ and $\lambda_{em,0-1}$ peaks of **1** and **3** are red-shifted vs those of [Ir(**L1**)$_2$(*d*tBubpy)][PF_6], whereas the $\lambda_{em,0-0}$ and $\lambda_{em,0-1}$ peaks of **2** and **4** appear nearly at the same energy compared to those of [Ir(**L1**)$_2$(*d*tBubpy)][PF_6] (see Table 2 for λ_{em} of **1**−**4**). Both the $\lambda_{em,0-0}$ and $\lambda_{em,0-1}$ peaks of [Ir(**L2**)$_2$(*d*tBubpy)][PF_6] are, however, more blue-shifted in comparison to those of **1**−**4** (see Table 2 for λ_{em} of **1**−**4**).

The Φ_{PL} values vary widely between 15 and 79% (Table 2). The observed τ_e values are single component, pointing toward emission from a single species. Complexes **2** and **4**, where the $-SF_5$ EWG is positioned *para* to the Ir−$C_{C^\wedge N}$ bond, were found to be more brightly emissive with longer τ_e in comparison to those of complexes **1** and **3**, where the $-SF_5$ EWG is positioned *meta* to the Ir−$C_{C^\wedge N}$ bond. The calculated radiative (k_r) and nonradiative (k_{nr}) decay constants ($k_r = \Phi_{PL}/\tau_e$ and $k_{nr} = (k_r/\Phi_{PL}) - k_r$) are in the range of (2.31−4.29) × 10^5 and (0.69−13.09) × 10^5 s^{-1}, respectively. The higher Φ_{PL} values of **2** vs **1** and **4** vs **3** are supported by the decrease in nonradiative decay by 19 and 4 times, respectively. The low Φ_{PL} values and high k_{nr} rates observed for complexes **1** and **3** may be explained by considering the deactivation of the emissive excited state through vibrational modes of the S−F bonds in the $-SF_5$ group that is *meta* to the Ir−$C_{C^\wedge N}$ bond, as we[49] had previously observed in a cationic iridium complex containing a $-CF_3$-substituted guanidylpyridine ancillary ligand. Frequency calculations of complexes **1** and **2** suggest that there is a strong coupling between the wagging mode of the C^N ligand with the wagging mode of the equatorial S−F bonds of the $-SF_5$ group in complex **1** (vibrational modes 46 and 47; E_{v46} = 322.59 cm^{-1} and E_{v47} = 324.23 cm^{-1}; cf. Table S9 in the Supporting Information for other minor contributing vibrational modes that couple with the spin density). These couplings are found to be very weakly present in complex **2**, as the $-SF_5$ group is in the *para* position in this complex and is therefore farther away from the $C_{C^\wedge N}$−Ir bond. A similar observation is found for the homoleptic complexes **3** and **4**. The principal vibrational modes of deactivation of the excited state of complex **3** are 90 (E_{v90} = 647.11 cm^{-1}) and 116 (E_{v116} = 865.29 cm^{-1}), where the asymmetric stretching modes of the $C_{C^\wedge N}$−$C_{C^\wedge N}$ bonds and Ir−$N_{C^\wedge N}$ bonds couple with the rocking mode of the equatorial S−F bonds and the equatorial out-of-plane vibration of the S atom of the $-SF_5$ group (cf. Table S10 in the Supporting Information for other minor contributing vibrational modes that couple with the spin density). Similar to what was observed for **2**, these deactivation modes are less pronounced in complex **4**, where the $-SF_5$ group is *para* to the $C_{C^\wedge N}$−Ir bond.

In order to assess their potential as emitters in OLEDs, the PL properties of **1**−**4** were investigated as doped PMMA thin films (PMMA = poly(methyl methacrylate)). The sample films were fabricated by spin-coating 5 wt % of the emitter in PMMA in chlorobenzene solutions in air. In doped thin films, the complexes exhibit phosphorescence behavior similar to that in solution with Φ_{PL} values of 23−51% (Figure 5b and Table 3). The emission maxima of **1**−**4** in doped films are similar to those in solution. In the case of **1**−**4**, the C^N ligands mainly contribute to the T_1 states, as shown in Figure 6, and thus the changes of the molecular dipole orientation are relatively small upon photoexcitation. As the PMMA molecules around the iridium complexes do not change their dipoles in the solid state, the nature of the T_1 states remains unchanged, unlike the positive rigidochromic effect observed by Ikawa et al.[28] for iridium complexes containing an O^O-based aromatic ancillary

DOI: 10.1021/acs.inorgchem.7b01075
Inorg. Chem. 2017, 56, 7533−7544

ligand where the T_1 state changes in nature. Enhancement in Φ_{PL} values of complexes **1** and **3** are observed in doped films in comparison to those in solution, while that of complex **2** decreases dramatically in the doped film. Complex **4** is virtually as efficient in the solid state (Φ_{PL} = 51%) as in MeCN solution (Φ_{PL} = 58%). The combination of molecular design, bulky $-SF_5$ groups on the C^N ligands and the *tert*-butyl groups of the thd ligand, and dispersion in PMMA that prevents intermolecular interactions of **1**−**4** makes the cause for the decrease in the Φ_{PL} of **2** unclear at present.

■ CONCLUSIONS

In summary, four new neutral iridium(III) complexes bearing strongly electron withdrawing pentafluorosulfanyl groups on the cyclometalating ligands have been synthesized and structurally characterized, including by single-crystal X-ray diffraction. Their photophysical properties have been investigated, and the complexes have been found to display sky blue to blue-green emission (λ_{em} 484−537 nm). Complexes **1**, **3**, and **4** exhibit quasi-reversible oxidation and irreversible reduction waves, while for complex **2** the first reduction takes place on the pyridyl moiety of the C^N ligands instead of the $-SF_5$ groups for the other three complexes. The trend in the red shift of the optical gap is in line with the regiochemistry of the $-SF_5$ EWG with respect to the Ir−C_{C^N} bond. The nature of the emission of these complexes is an admixture of ^{3}LC and ^{3}MLCT, corroborated by DFT calculations, and the predicted emission maximum follows the trend of the experimental values of respective complexes. While complexes **1** and **3**, bearing $-SF_5$ EWG *meta* to the Ir−C_{C^N} bond of the C^N ligand, exhibit red-shifted emission in comparison to mono-/difluoro analogues (**1** vs **R5**/**R6** and **3** vs **R9**/**R10**), complexes **2** and **4**, which are substituted by $-SF_5$ *para* to the Ir−C_{C^N} bond of the C^N ligand, display blue-shifted $\lambda_{em,0-0}$ in comparison to their mono-/difluoro analogues (**2** vs **R5**/**R6** and **4** vs **R9**). Thus, this study demonstrates the value of introduction of a pentafluorosulfanyl group onto the C^N ligands *para* to the Ir−C_{C^N} bond to promote a greater blue shift in the emission in comparison to the commonly employed dFppy ligands. The photophysical data of these emitters (λ_{em} 480−531 nm; Φ_{PL} = 23−51%) on dispersion at a concentration of 5 wt % in PMMA thin films suggest that these complexes would be of interest as sky blue emitter replacements for commonly used phosphors, such as FIrpic, [Ir(dFppy)(pic)]. Current efforts are underway to evaluate them in OLEDs.

■ EXPERIMENTAL SECTION

General Synthetic Procedures. Commercial chemicals were used without further purification. Ligands **HL1** and **HL2** were synthesized using a literature procedure.[26] All reactions were performed using standard Schlenk techniques under an inert (N_2) atmosphere with reagent grade solvents. Flash column chromatography was performed using silica gel (60 Å, 40−63 μm). Silica plates with aluminum backings (250 μm with indicator F-254) were used for analytical thin layer chromatography (TLC). Compounds were visualized under UV irradiation. ^{1}H (for ligands and dimers), ^{13}C, and ^{19}F NMR spectra were recorded on a Bruker Avance spectrometer at 400, 125, and 376 MHz, respectively. The following abbreviations have been used for multiplicity assignments: "s" for singlet, "d" for doublet, "t" for triplet, "p" for pentet, "m" for multiplet, and "br" for broad. Deuterated chloroform ($CDCl_3$) and deuterated dichloromethane (CD_2Cl_2) were used as the solvents of record. ^{1}H and ^{13}C NMR spectra were referenced with respect to the NMR solvent peaks. An Electrothermal melting point apparatus was used to record melting points (mps). Mps were recorded in open-ended capillaries and are uncorrected. Thermogravimetric analysis (TGA) data were collected on a TA Instruments SDT 2960 apparatus. High-resolution mass spectra (HRMS) were recorded at the EPSRC UK National Mass Spectrometry Facility at Swansea University on a quadrupole time-of-flight (Q-TOF) instrument using a Model ABSciex 5600 Triple TOF in positive electrospray ionization (pESI) mode, and spectra were recorded using sodium formate solution as the calibrant. Elemental analyses were performed by Mr. Stephen Boyer, London Metropolitan University.

Syntheses of Precursor [Ir(C^N)$_2$(μ-Cl)]$_2$ Dimers D1 and D2. The dimers were synthesized following literature procedures.[25]

*Tetrakis[2-(4-(pentafluoro-λ^6-sulfanyl)phenyl)pyridinato-N,C$^{2'}$]-bis(μ-chloro)diiridium(III), [Ir(**L1**)$_2$(μ-Cl)]$_2$ (**D1**).* $IrCl_3 \cdot 3H_2O$ (0.2 g, 0.57 mmol, 1 equiv) and **HL1** (0.36 g, 1.3 mmol, 2.28 equiv) in a degassed mixture of 2-ethoxyethanol (6 mL) and water (2 mL) affords the dimer **D1** as yellow solid. Yield: 0.41 g, 91%. ^{1}H NMR (400 MHz, $CDCl_3$, main component) δ (ppm): 9.23−9.19 (m, 4H), 8.01−7.97 (m, 4H), 7.92 (td, *J* = 7.4, 1.5 Hz, 4H), 7.58 (d, *J* = 8.6 Hz, 4H), 7.22 (d, *J* = 8.6, 2.2 Hz, 4H), 6.97 (ddd, *J* = 7.3, 5.8, 1.5 Hz, 4H), 6.12 (d, *J* = 2.2 Hz, 4H). ^{19}F{^{1}H} NMR (377 MHz, $CDCl_3$, main component) δ (ppm): 84.9 (p, *J* = 151 Hz, 4F), 61.7 (d, *J* = 151 Hz, 16F). The characterization data match those previously reported.[26]

*Tetrakis[2-(3-(pentafluoro-λ^6-sulfanyl)phenyl)pyridinato-N,C$^{2'}$]-bis(μ-chloro)diiridium(III), [Ir(**L2**)$_2$(μ-Cl)]$_2$ (**D2**).* $IrCl_3 \cdot 3H_2O$ (0.2 g, 0.57 mmol, 1 equiv) and **HL2** (0.36 g, 1.3 mmol, 2.28 equiv) in a degassed mixture of 2-ethoxyethanol (6 mL) and water (2 mL) affords the dimer D2 as a yellow solid. Yield: 0.38 g, 85%. ^{1}H NMR (400 MHz, $CDCl_3$, main component) δ (ppm): 9.17 (dd, *J* = 5.8, 0.8 Hz, 4H), 8.01 (d, *J* = 7.8 Hz, 4H), 7.91 (td, *J* = 7.5, 1.5 Hz, 4H), 7.86 (d, *J* = 2.4 Hz, 4H), 6.97 (dd, *J* = 8.7, 2.4 Hz, 4H), 6.93 (ddd, *J* = 7.3, 5.8, 1.4 Hz, 4H), 5.96 (d, *J* = 8.6 Hz, 4H). ^{19}F{^{1}H} NMR (377 MHz, $CDCl_3$, main component) δ (ppm): 85.9 (p, *J* = 151 Hz, 4F), 63.0 (d, *J* = 150 Hz, 16F). The characterization data match those previously reported.[26]

Syntheses of [Ir(C^N)$_2$(thd)] (1 and 2) and [Ir(C^N)$_3$] (3 and 4) Complexes. *Bis[2-(4-(pentafluoro-λ^6-sulfanyl)phenyl)pyridinato-N,C$^{2'}$](2,2,6,6-tetramethylheptane-3,5-dionato-κO^3,κO^6)iridium(III), [Ir(**L1**)$_2$(thd)] (**1**).* The reaction was performed under nitrogen. The precursor dimer complex [Ir(**L1**)$_2$(μ-Cl)]$_2$ (150 mg, 0.095 mmol, 1 equiv), anhydrous Na_2CO_3 (25 mg, 0.24 mmol, 2.53 equiv), and 2,2,6,6-tetramethyl-3,5-heptanedione (54 mg, 0.29 mmol, 3.05 equiv) were stirred in degassed 2-methoxyethanol (4 mL) at 110 °C for 24 h to give an orange mixture. The mixture was cooled to room temperature, and water (50 mL) was added. The suspension was stirred for 10 min and filtered. The solid product was washed with water and with methanol/water (2/1, v/v) and was then purified by column chromatography on silica (17 g; 40−63 μm). The elution was performed with hexane/dichloromethane (1/1, v/v) to give a yellow fraction. The solution was evaporated to dryness. The product still contained the starting ligand. Therefore, the product was dissolved in methanol (17 mL), and it was precipitated on stirring with water (8.5 mL). The product was filtered and washed with methanol/water (2/1, v/v). Orange solid. Yield: 113 mg, 64%. R_f: 0.51 (hexanes/DCM: 3/2, v/v, on silica). Mp: 254−255 °C. TGA: >350 °C (5% decomposition). ^{1}H NMR (400 MHz, CD_2Cl_2) δ (ppm): 8.39 (ddd, *J* = 5.7, 1.5, 0.8 Hz, 2H), 7.96 (d, *J* = 7.9 Hz, 2H), 7.89−7.83 (m, 2H), 7.67 (d, *J* = 8.6 Hz, 2H), 7.30−7.24 (m, 4H), 6.56 (d, *J* = 2.3 Hz, 2H), 5.57 (s, 1H), 0.90 (s, 18H). ^{13}C NMR (125 MHz, CD_2Cl_2) δ (ppm): 195.60, 166.77, 149.26, 149.11, 148.88, 138.39, 129.45, 128.96, 123.92, 123.64, 120.10, 118.87, 90.83, 41.60, 28.32. ^{19}F{^{1}H} NMR (377 MHz, CD_2Cl_2) δ (ppm): 86.3 (p, *J* = 149 Hz, 2F), 62.2 (d, *J* = 149 Hz, 8F). HR APCI$^+$ **MS**: $[M + H]^+$ (100%) calcd 937.1524, ($C_{33}H_{34}F_{10}IrN_2O_2S_2^+$); found 937.1543. Anal. Calcd for $C_{33}H_{33}F_{10}IrN_2O_2S_2$: C, 42.35; H, 3.55; N, 2.99. Found: C, 42.45; H, 3.50; N, 3.03.

*Bis[2-(3-(pentafluoro-λ^6-sulfanyl)phenyl)pyridinato-N,C$^{2'}$]-(2,2,6,6-tetramethylheptane-3,5-dionato-κO^3,κO^6)iridium(III), [Ir(**L2**)$_2$(thd)] (**2**).* The reaction was performed under nitrogen. The precursor dimer complex [Ir(**L2**)$_2$(μ-Cl)]$_2$ (150 mg, 0.095 mmol, 1 equiv), anhydrous Na_2CO_3 (25 mg, 0.24 mmol, 2.53 equiv), and

DOI: 10.1021/acs.inorgchem.7b01075
Inorg. Chem. 2017, 56, 7533−7544

2,2,6,6-tetramethyl-3,5-heptanedione (60 mg, 0.33 mmol, 3.47 equiv) were stirred in degassed 2-methoxyethanol (4 mL) at 110 °C for 24 h to give a yellow mixture. The mixture was cooled to room temperature, and water (50 mL) was added. The suspension was stirred for 10 min and filtered. The solid product was washed with water and with methanol/water (2/1, v/v) and was then purified by column chromatography on silica (17 g, 40−63 μm). The elution was performed with hexane/dichloromethane (1/2, v/v) to give a yellow fraction. The solution was evaporated to dryness. The glassy product was suspended in methanol (10 mL) and sonicated for 1 min. The product is not very soluble in methanol. Water was added (5 mL). The mixture was sonicated again for 1 min. The product was filtered and washed with methanol/water (2/1, v/v). Yellow solid. Yield: 149 mg, 84%. R_f: 0.57 (hexanes/DCM: 3/2, v/v, on silica). Mp: 324−325 °C dec. TGA: 98 °C (5% decomposition). ^{1}H NMR (400 MHz, CD_2Cl_2) δ (ppm): 8.38 (ddd, J = 5.7, 1.5, 0.8 Hz, 2H), 7.97−7.91 (m, 4H), 7.89−7.83 (m, 2H), 7.25 (ddd, J = 7.3, 5.7, 1.4 Hz, 2H), 7.03 (dd, J = 8.5, 2.4 Hz, 2H), 6.44 (d, J = 8.5 Hz, 2H), 5.59 (s, 1H), 0.90 (s, 18H). ^{13}C NMR (125 MHz, CD_2Cl_2) δ (ppm): 195.66, 167.10, 156.07, 148.95, 145.97, 138.35, 133.75, 128.96, 125.63, 123.29, 120.91, 119.46, 90.82, 41.61, 28.33. ^{19}F{^{1}H} NMR (377 MHz, CD_2Cl_2) δ (ppm): 87.4 (p, J = 149 Hz, 2F), 63.7 (d, J = 149 Hz, 8F). HR APCI$^+$ MS: [M + H]$^+$ (100%) calcd 937.1524, ($C_{33}H_{34}F_{10}IrN_2O_2S_2^+$); found 937.1535. Anal. Calcd for $C_{33}H_{33}F_{10}IrN_2O_2S_2$: C, 42.35; H, 3.55; N, 2.99. Found: C, 42.21; H, 3.44; N, 2.91.

General Procedure for the Synthesis of *fac*-[Ir(C^N)$_3$] Complexes. In a round-bottom flask containing Ir(acac)$_3$ (1.0 equiv) and C^N ligand (3.1 equiv) was placed ethylene glycol to give a suspension with a concentration of ca. 0.3 M. The mixture was sealed and then degassed by repeated vacuum−N_2 cycles, before being placed under N_2. The reaction mixture was heated to reflux for 72 h. The mixture was then cooled to room temperature, and water was added. The mixture was then extracted with DCM and dried over $MgSO_4$ before filtering under reduced pressure. The material was then purified by column chromatography on silica gel, using first a hexanes/Et_2O mixture (80/20, v/v) to remove the ligand and then DCM or DCM/MeOH (95/5, v/v) to elute the complex. For both complexes ^{19}F NMR indicated the presence of a small impurity, which was assigned as the *mer* isomer given the microanalysis.

*fac-Tris[2-(4′-pentafluorosulfanyl)-pyridinato-N,C$^{2'}$]iridium(III), fac-[Ir(**L1**)$_3$] (**3**).* Column conditions: DCM. Yellow powder. Yield: 0.111 g, 42%. R_f: 0.80 (hexanes/DCM: 2/3, v/v, on silica). Mp: 375 °C dec. TGA: 217 °C (5% decomposition). ^{1}H{^{19}F} NMR (400 MHz, CD_2Cl_2) δ (ppm): 8.01 (d, J = 8.2, Hz, 3H), 7.80 (td, J = 8.1, 1.6 Hz, 3H), 7.79 (d, J = 8.6 Hz, 3H), 7.61 (dd, J = 5.6, 0.8 Hz, 3H), 7.33 (dd, J = 8.6, 2.4 Hz, 3H), 7.11 (ddd, J = 7.0, 5.6, 1.3 Hz, 3H), 7.01 (d, J = 2.4 Hz, 3H). ^{13}C NMR (125 MHz, CD_2Cl_2) δ (ppm): 164.7, 159.2, 147.9, 147.4, 137.8, 132.8, 124.4, 124.3, 120.8, 118.5 (one quaternary ^{13}C NMR signal was found to be missing). ^{19}F{^{1}H} NMR (377 MHz, CD_2Cl_2) δ (ppm): 85.85 (p, J = 148.77 Hz, 3F), 61.90 (d, J = 148.77 Hz, 12F). HR-MS (TOF MS ASAP+): [M + H]$^+$ (100%) calcd 1034.0367, ($C_{33}H_{22}N_3F_{15}S_3Ir^+$); found 1034.0363. Anal. Calcd for $C_{33}H_{21}N_3F_{15}S_3Ir$ (MW 1032.93): C, 38.37; H, 2.05; N, 4.07. Found: C, 38.61; H, 2.36; N, 3.86 (average of two runs).

*fac-Tris[2-(5′-pentafluorosulfanyl)-pyridinato-N,C$^{2'}$]iridium(III), fac-[Ir(**L2**)$_3$] (**4**).* Column conditions: DCM/MeOH (95/5, v/v). Yellow powder. Yield: 0.163 g, 78%. R_f: 0.87 (hexanes/DCM: 2/3, v/v, on silica). Mp: 345 °C dec. TGA: 157 °C (5% decomposition). ^{1}H{^{19}F} NMR (400 MHz, CD_2Cl_2) δ (ppm): 8.03−7.98 (m, 6H), 7.80 (ddd, J = 8.2, 7.4, 1.6 Hz, 3H), 7.55 (ddd, J = 5.5, 1.7, 0.8 Hz, 3H), 7.16 (dd, J = 8.5, 2.4 Hz, 3H), 7.08 (ddd, J = 7.3, 5.6, 1.2 Hz, 3H), 6.84 (d, J = 8.5 Hz, 3H). ^{13}C NMR (125 MHz, CD_2Cl_2) δ (ppm): 165.7, 164.8, 147.8, 144.6, 137.9, 136.8, 126.6, 124.1, 121.3, 120.1 (one quaternary ^{13}C NMR signal was found to be missing). ^{19}F{^{1}H} NMR (377 MHz, CD_2Cl_2) δ (ppm): 87.57 (p, J = 149.53 Hz, 3F), 63.63 (d, J = 149.53 Hz, 12F). HR-MS (TOF MS NSI+): [M + H]$^+$ (100%) calcd 1034.0367 ($C_{33}H_{22}N_3F_{15}S_3Ir^+$); found 1034.0364. Anal. Calcd for $C_{33}H_{21}N_3F_{15}S_3Ir$ (MW 1032.93): C, 38.37; H, 2.05; N, 4.07. Found: C, 38.61; H, 2.36; N, 3.86 (average of two runs).

X-ray Crystallography. Single crystals were grown by diffusion of an anti-solvent (**1**, ethanol; **2**, methanol; **3**, diethyl ether; **4**, hexane) into concentrated solutions of the complexes in dichloromethane (CCDC: 1527433−1527436). Crystallographic techniques similar to those found in the study of Pal et al. was adopted to determine the solid-state structures.[25] Structures were solved by Patterson (PATTY; **1**, **3**),[52] direct (SIR2004; **2**),[53] or dual-space (SHELXT; **4**)[54] methods and refined by full-matrix least squares against F^2 (SHELXL-2013).[54]

Photophysical Measurements. HPLC grade MeCN was used to prepare sample solutions with varying concentrations in the order of micromoles. Detailed techniques of UV−vis spectroscopy, steady-state, time-resolved photoluminescence spectroscopy, determination of photoluminescence quantum yields by optical dilution method,[55,56] and respective instruments used were the same as found in the study of Pal et al.[25]

Electrochemistry Measurements. Cyclic voltammetry (CV) and differential pulse voltammetry (DPV) measurements were performed following the procedure in the study of Pal et al.[25]

Estimated uncertainties on measurements: UV−vis absorption spectra, ± 2 nm; molar extinction coefficients, 10%; CV and DPV redox potentials, ±10 mV; steady-state emission spectra, ±3 nm; excited state lifetimes, ±10%; photoluminescence quantum yields, ±5%.

ASSOCIATED CONTENT

Supporting Information

The Supporting Information is available free of charge on the ACS Publications website at DOI: 10.1021/acs.inorgchem.7b01075. The research data supporting this work can be accessed at: http://dx.doi.org/10.17630/6da56570-6be6-4931-9a72-63144c352b0a.

NMR spectra of all C^N ligands, dimers, and complexes and supplementary optoelectronic and DFT data of complexes **1**−**4** (PDF)

Accession Codes

CCDC 1527433−1527436 contain the supplementary crystallographic data for this paper. These data can be obtained free of charge via www.ccdc.cam.ac.uk/data_request/cif, or by emailing data_request@ccdc.cam.ac.uk, or by contacting The Cambridge Crystallographic Data Centre, 12 Union Road, Cambridge CB2 1EZ, UK; fax: +44 1223 336033.

AUTHOR INFORMATION

Corresponding Author

*E.Z.-C.: fax, +44-1334 463808; tel, +44-1334 463826; e-mail, eli.zysman-colman@st-andrews.ac.uk; web, http://www.zysman-colman.com.

ORCID

Eli Zysman-Colman: 0000-0001-7183-6022

Author Contributions

‖A.K.P. and A.F.H. contributed equally.

Notes

The authors declare no competing financial interest.

ACKNOWLEDGMENTS

E.Z.-C. acknowledges the University of St Andrews for financial support. We thank the EPSRC UK National Mass Spectrometry Facility at Swansea University for analytical services. We are grateful to the EPSRC for financial support from grant EP/M02105X/1, DTG grants: EP/J500549/1, EP/K503162/1, EP/L505097/1. We are grateful to the European Research Council (grant 321305) for support. I.D.W.S. is a Royal Society Wolfon Research Merit Award holder. We thank Umicore AG for the gift of materials. We thank Dr. Nail Shavaleev for the synthesis of the complexes **1** and **2** in this study.

REFERENCES

(1) Kalyanasundaram, K.; Grätzel, M. Applications of functionalized transition metal complexes in photonic and optoelectronic devices. *Coord. Chem. Rev.* **1998**, *177*, 347.

(2) Lees, A. J. Luminescence properties of organometallic complexes. *Chem. Rev.* **1987**, *87*, 711.

(3) For recent reviews see: Flamigni, L.; Barbieri, A.; Sabatini, C.; Ventura, B.; Barigelletti, F. Photochemistry and Photophysics of Coordination Compounds: Iridium. *Top. Curr. Chem.* **2007**, *281*, 143.

(4) Ulbricht, C.; Beyer, B.; Friebe, C.; Winter, A.; Schubert, U. S. Recent Developments in the Application of Phosphorescent Iridium(III) Complex Systems. *Adv. Mater.* **2009**, *21*, 4418.

(5) Farinola, G. M.; Ragni, R. Electroluminescent materials for white organic light emitting diodes. *Chem. Soc. Rev.* **2011**, *40*, 3467.

(6) Zhou, G.; Wong, W.-Y.; Suo, S. Recent progress and current challenges in phosphorescent white organic light-emitting diodes (WOLEDs). *J. Photochem. Photobiol., C* **2010**, *11*, 133.

(7) Costa, R. D.; Ortí, E.; Bolink, H. J.; Monti, F.; Accorsi, G.; Armaroli, N. Luminescent Ionic Transition-Metal Complexes for Light-Emitting Electrochemical Cells. *Angew. Chem., Int. Ed.* **2012**, *51*, 8178.

(8) Lo, K. K.-W.; Zhang, K. Y. Iridium(iii) complexes as therapeutic and bioimaging reagents for cellular applications. *RSC Adv.* **2012**, *2*, 12069.

(9) Lo, K. K.-W.; Tso, K. K.-S. Functionalization of cyclometalated iridium(iii) polypyridine complexes for the design of intracellular sensors, organelle-targeting imaging reagents, and metallodrugs. *Inorg. Chem. Front.* **2015**, *2*, 510.

(10) Ma, D.-L.; Lin, S.; Wang, W.; Yang, C.; Leung, C.-H. Luminescent chemosensors by using cyclometalated iridium(iii) complexes and their applications. *Chem. Sci.* **2017**, *8*, 878.

(11) He, L.; Duan, L.; Qiao, J.; Wang, R.; Wei, P.; Wang, L.; Qiu, Y. Blue-Emitting Cationic Iridium Complexes with 2-(1H-Pyrazol-1-yl)pyridine as the Ancillary Ligand for Efficient Light-Emitting Electrochemical Cells. *Adv. Funct. Mater.* **2008**, *18*, 2123.

(12) He, L.; Duan, L.; Qiao, J.; Dong, G.; Wang, L.; Qiu, Y. Highly Efficient Blue-Green and White Light-Emitting Electrochemical Cells Based on a Cationic Iridium Complex with a Bulky Side Group. *Chem. Mater.* **2010**, *22*, 3535.

(13) Mydlak, M.; Bizzarri, C.; Hartmann, D.; Sarfert, W.; Schmid, G.; De Cola, L. Positively Charged Iridium(III) Triazole Derivatives as Blue Emitters for Light-Emitting Electrochemical Cells. *Adv. Funct. Mater.* **2010**, *20*, 1812.

(14) Axtell, J. C.; Kirlikovali, K. O.; Djurovich, P. I.; Jung, D.; Nguyen, V. T.; Munekiyo, B.; Royappa, A. T.; Rheingold, A. L.; Spokoyny, A. M. Blue Phosphorescent Zwitterionic Iridium(III) Complexes Featuring Weakly Coordinating nido-Carborane-Based Ligands. *J. Am. Chem. Soc.* **2016**, *138*, 15758.

(15) Sivasubramaniam, V.; Brodkorb, F.; Hanning, S.; Loebl, H. P.; van Elsbergen, V.; Boerner, H.; Scherf, U.; Kreyenschmidt, M. Fluorine cleavage of the light blue heteroleptic triplet emitter FIrpic. *J. Fluorine Chem.* **2009**, *130*, 640.

(16) Constable, E. C.; Ertl, C. D.; Housecroft, C. E.; Zampese, J. A. Green-emitting iridium(iii) complexes containing sulfanyl- or sulfone-functionalized cyclometallating 2-phenylpyridine ligands. *Dalton Trans.* **2014**, *43*, 5343.

(17) Ragni, R.; Orselli, E.; Kottas, G. S.; Omar, O. H.; Babudri, F.; Pedone, A.; Naso, F.; Farinola, G. M.; De Cola, L. Iridium(III) complexes with sulfonyl and fluorine substituents: synthesis, stereochemistry and effect of functionalisation on their photophysical properties. *Chem. - Eur. J.* **2009**, *15*, 136.

(18) Zhou, G.; Wang, Q.; Ho, C. L.; Wong, W. Y.; Ma, D.; Wang, L.; Lin, Z. Robust tris-cyclometalated iridium(III) phosphors with ligands for effective charge carrier injection/transport: synthesis, redox, photophysical, and electrophosphorescent behavior. *Chem. - Asian J.* **2008**, *3*, 1830.

(19) Grushin, V. V.; Herron, N.; LeCloux, D. D.; Marshall, W. J.; Petrov, V. A.; Wang, Y. New, efficient electroluminescent materials based on organometallic Ir complexes. *Chem. Commun.* **2001**, 1494.

(20) Coppo, P.; Plummer, E. A.; De Cola, L. Tuning iridium(iii) phenylpyridine complexes in the ″almost blue″ region. *Chem. Commun.* **2004**, 1774.

(21) Liu, C.; Lv, X.; Xing, Y.; Qiu, J. Trifluoromethyl-substituted cyclometalated iridiumIIIemitters with high photostability for continuous oxygen sensing. *J. Mater. Chem. C* **2015**, *3*, 8010.

(22) Singh, A.; Teegardin, K.; Kelly, M.; Prasad, K. S.; Krishnan, S.; Weaver, J. D. Facile synthesis and complete characterization of homoleptic and heteroleptic cyclometalated Iridium(III) complexes for photocatalysis. *J. Organomet. Chem.* **2015**, *776*, 51.

(23) Tao, P.; Li, W.-L.; Zhang, J.; Guo, S.; Zhao, Q.; Wang, H.; Wei, B.; Liu, S.-J.; Zhou, X.-H.; Yu, Q.; Xu, B.-S.; Huang, W. Facile Synthesis of Highly Efficient Lepidine-Based Phosphorescent Iridium(III) Complexes for Yellow and White Organic Light-Emitting Diodes. *Adv. Funct. Mater.* **2016**, *26*, 881.

(24) Shavaleev, N. M.; Monti, F.; Scopelliti, R.; Armaroli, N.; Grätzel, M.; Nazeeruddin, M. K. Blue Phosphorescence of Trifluoromethyl- and Trifluoromethoxy-Substituted Cationic Iridium(III) Isocyanide Complexes. *Organometallics* **2012**, *31*, 6288.

(25) Pal, A. K.; Cordes, D. B.; Slawin, A. M. Z.; Momblona, C.; Ortí, E.; Samuel, I. D. W.; Bolink, H. J.; Zysman-Colman, E. Synthesis, Properties, and Light-Emitting Electrochemical Cell (LEEC) Device Fabrication of Cationic Ir(III) Complexes Bearing Electron-Withdrawing Groups on the Cyclometallating Ligands. *Inorg. Chem.* **2016**, *55*, 10361.

(26) Shavaleev, N. M.; Xie, G.; Varghese, S.; Cordes, D. B.; Slawin, A. M. Z.; Momblona, C.; Ortí, E.; Bolink, H. J.; Samuel, I. D. W.; Zysman-Colman, E. Green Phosphorescence and Electroluminescence of Sulfur Pentafluoride-Functionalized Cationic Iridium(III) Complexes. *Inorg. Chem.* **2015**, *54*, 5907.

(27) Lamansky, S.; Djurovich, P.; Murphy, D.; Abdel-Razzaq, F.; Lee, H.-E.; Adachi, C.; Burrows, P. E.; Forrest, S. R.; Thompson, M. E. Highly Phosphorescent Bis-Cyclometalated Iridium Complexes: Synthesis, Photophysical Characterization, and Use in Organic Light Emitting Diodes. *J. Am. Chem. Soc.* **2001**, *123*, 4304.

(28) Ikawa, S.; Yagi, S.; Maeda, T.; Nakazumi, H.; Fujiwara, H.; Sakurai, Y. Photoluminescence color tuning of phosphorescent bis-cyclometalated iridium(III) complexes by ancillary ligand replacement. *Dyes Pigm.* **2012**, *95*, 695.

(29) Frey, J.; Curchod, B. F. E.; Scopelliti, R.; Tavernelli, I.; Rothlisberger, U.; Nazeeruddin, M. K.; Baranoff, E. Structure-property relationships based on Hammett constants in cyclometalated iridium(iii) complexes: their application to the design of a fluorine-free FIrPic-like emitter. *Dalton Trans.* **2014**, *43*, 5667.

(30) Lepeltier, M.; Morlet-Savary, F.; Graff, B.; Lalevée, J.; Gigmes, D.; Dumur, F. Efficient blue green organic light-emitting devices based on a monofluorinated heteroleptic iridium(III) complex. *Synth. Met.* **2015**, *199*, 139.

(31) Takayasu, S.; Suzuki, T.; Shinozaki, K. Intermolecular interactions and aggregation of fac-tris(2-phenylpyridinato-C2,N)-iridium(III) in nonpolar solvents. *J. Phys. Chem. B* **2013**, *117*, 9449.

(32) Hansch, C.; Leo, A.; Taft, R. W. A survey of Hammett substituent constants and resonance and field parameters. *Chem. Rev.* **1991**, *91*, 165.

(33) Recent reviews: Jackson, D. A.; Mabury, S. A. Environmental properties of pentafluorosulfanyl compounds: Physical properties and photodegradation. *Environ. Toxicol. Chem.* **2009**, *28*, 1866.

(34) Altomonte, S.; Zanda, M. Synthetic chemistry and biological activity of pentafluorosulphanyl (SF5) organic molecules. *J. Fluorine Chem.* **2012**, *143*, 57.

(35) Savoie, P. R.; Welch, J. T. Preparation and Utility of Organic Pentafluorosulfanyl-Containing Compounds. *Chem. Rev.* **2015**, *115*, 1130.

(36) Jacquemin, D.; Planchat, A.; Adamo, C.; Mennucci, B. TD-DFT Assessment of Functionals for Optical 0–0 Transitions in Solvated Dyes. *J. Chem. Theory Comput.* **2012**, *8*, 2359.

DOI: 10.1021/acs.inorgchem.7b01075
Inorg. Chem. 2017, 56, 7533–7544

(37) Escudero, D.; Jacquemin, D. Computational insights into the photodeactivation dynamics of phosphors for OLEDs: a perspective. *Dalton Trans.* **2015**, *44*, 8346.
(38) Kim, T.; Kim, H.; Lee, K. M.; Lee, Y. S.; Lee, M. H. Phosphorescence color tuning of cyclometalated iridium complexes by o-carborane substitution. *Inorg. Chem.* **2013**, *52*, 160.
(39) Stille, J. K. The Palladium-Catalyzed Cross-Coupling Reactions of Organotin Reagents with Organic Electrophiles [New Synthetic Methods (58)]. *Angew. Chem., Int. Ed. Engl.* **1986**, *25*, 508.
(40) Harrowven, D. C.; Curran, D. P.; Kostiuk, S. L.; Wallis-Guy, I. L.; Whiting, S.; Stenning, K. J.; Tang, B.; Packard, E.; Nanson, L. Potassium carbonate-silica: a highly effective stationary phase for the chromatographic removal of organotin impurities. *Chem. Commun.* **2010**, *46*, 6335.
(41) Nonoyama, M. Benzo[h]quinolin-10-yl-N Iridium(III) Complexes. *Bull. Chem. Soc. Jpn.* **1974**, *47*, 767.
(42) Tamayo, A. B.; Alleyne, B. D.; Djurovich, P. I.; Lamansky, S.; Tsyba, I.; Ho, N. N.; Bau, R.; Thompson, M. E. Synthesis and Characterization of Facial and Meridional Tris-cyclometalated Iridium(III) Complexes. *J. Am. Chem. Soc.* **2003**, *125*, 7377.
(43) Lee, J.; Chen, H.-F.; Batagoda, T.; Coburn, C.; Djurovich, P. I.; Thompson, M. E.; Forrest, S. R. Deep blue phosphorescent organic light-emitting diodes with very high brightness and efficiency. *Nat. Mater.* **2015**, *15*, 92.
(44) Eaton, D. R.; Sheppard, W. A. F19 Chemical Shifts of the Sulfur Pentafluoride, Trifluoromethoxy, Trifluoromethylthio and Trifluoromethylsulfonyl Groups in Aromatic Compounds. *J. Am. Chem. Soc.* **1963**, *85*, 1310.
(45) Pavlishchuk, V. V.; Addison, A. W. Conversion constants for redox potentials measured versus different reference electrodes in acetonitrile solutions at 25°C. *Inorg. Chim. Acta* **2000**, *298*, 97.
(46) Baranoff, E.; Curchod, B. F. E.; Frey, J.; Scopelliti, R.; Kessler, F.; Tavernelli, I.; Rothlisberger, U.; Grätzel, M.; Nazeeruddin, M. K. Acid-Induced Degradation of Phosphorescent Dopants for OLEDs and Its Application to the Synthesis of Tris-heteroleptic Iridium(III) Bis-cyclometalated Complexes. *Inorg. Chem.* **2012**, *51*, 215.
(47) Tian, N.; Lenkeit, D.; Pelz, S.; Fischer, L. H.; Escudero, D.; Schiewek, R.; Klink, D.; Schmitz, O. J.; González, L.; Schäferling, M.; Holder, E. Structure–Property Relationship of Red- and Green-Emitting Iridium(III) Complexes with Respect to Their Temperature and Oxygen Sensitivity. *Eur. J. Inorg. Chem.* **2010**, *2010*, 4875.
(48) Lamansky, S.; Djurovich, P.; Murphy, D.; Abdel-Razzaq, F.; Kwong, R.; Tsyba, I.; Bortz, M.; Mui, B.; Bau, R.; Thompson, M. E. Synthesis and Characterization of Phosphorescent Cyclometalated Iridium Complexes. *Inorg. Chem.* **2001**, *40*, 1704.
(49) Sajjad, M. T.; Sharma, N.; Pal, A. K.; Hasan, K.; Xie, G.; Kölln, L. S.; Hanan, G. S.; Samuel, I. D. W.; Zysman-Colman, E. Controlling the emission efficiency of blue-green iridium(iii) phosphorescent emitters and applications in solution-processed organic light-emitting diodes. *J. Mater. Chem. C* **2016**, *4*, 8939.
(50) Melhuish, W. H. Quantum Efficiences Of Fluorescence Of Organic Substances: Effect Of Solvent And Concentration Of The Fluorescent Solute 1. *J. Phys. Chem.* **1961**, *65*, 229.
(51) Tian, N.; Lenkeit, D.; Pelz, S.; Kourkoulos, D.; Hertel, D.; Meerholz, K.; Holder, E. Screening structure-property correlations and device performance of Ir(III) complexes in multi-layer PhOLEDs. *Dalton Trans* **2011**, *40*, 11629.
(52) Beurskens, P. T.; Beurskens, G.; de Gelder, R.; Garcia-Granda, S.; Gould, R. O.; Israel, R.; Smits, J. M. M. *DIRDIF-99*; University of Nijmegen, Nijmegen, The Netherlands, 1999.
(53) Burla, M. C.; Caliandro, R.; Camalli, M.; Carrozzini, B.; Cascarano, G. L.; De Caro, L.; Giacovazzo, C.; Polidori, G.; Spagna, R. SIR2004: an improved tool for crystal structure determination and refinement. *J. Appl. Crystallogr.* **2005**, *38*, 381.
(54) Sheldrick, G. Crystal structure refinement with SHELXL. *Acta Crystallogr., Sect. C: Struct. Chem.* **2015**, *71*, 3.
(55) Crosby, G. A.; Demas, J. N. Measurement of photoluminescence quantum yields. Review. *J. Phys. Chem.* **1971**, *75*, 991.
(56) Brouwer, A. M. Standards for photoluminescence quantum yield measurements in solution (IUPAC Technical Report)*. *Pure Appl. Chem.* **2011**, *83*, 2213.

DOI: 10.1021/acs.inorgchem.7b01075
Inorg. Chem. 2017, 56, 7533−7544